

Original article

Pore-scale remaining oil distribution under different pore volume water injection based on CT technology

Zhihui Liu¹, Yongfei Yang^{1*}, Jun Yao¹, Qi Zhang¹, Jingsheng Ma², Qihao Qian³

¹Research Centre of Multiphase Flow in Porous Media, China University of Petroleum (East China), Qingdao 266580, P. R. China

²Institute of Petroleum Engineering, Heriot-Watt University, Riccarton, Edinburgh EH14 4AS, UK

³PetroChina Research Institute of Petroleum Exploration & Development, Beijing 100083, P. R. China

(Received October 15, 2017; revised November 4, 2017; accepted November 6, 2017; published December 25, 2017)

Abstract: A water-injection experiment was performed on a water-wet reservoir core plug that was filled with brine first and then displaced by synthetic oil. A X-ray Computed Tomography was used to take snapshots of the process of oil-water displacement at predefined time intervals to characterize the distribution of remaining oil. The quasi-real time images were used to understand the pore-scale phase displacement mechanisms and the distributional pattern of the remaining oil. Four forms of the distributional patterns, i.e. network, porous, isolated and film shape, were observed and analyzed with respect to the injected pore volumes (PV). The results show that with the increased level of water injection, the volume of the oil phase continuously decreases, and the morphology of the oil phase changes from initial continuous network-like to film shape forms. At 15 PV, the network-like remaining oil disappears and transforms into isolated and film-like forms. The statistics of the volume for each form of the remaining oil show that the isolated blobs increase with increasing water injection, by contrast, the average volume of the remaining oil decreases with increasing water injection. The rate of volumetric changes is fast before 5 PV but slow in the later period.

Keywords: CT, pore scale, digital core, remaining oil distribution, quasi real time.

Citation: Liu, Z., Yang, Y., Yao, J., et al. Pore-scale remaining oil distribution under different pore volume water injection based on CT technology. *Adv. Geo-Energy Res.* 2017, 1(3): 171-181, doi: 10.26804/ager.2017.03.04.

1. Introduction

The recent release of BP “World Energy Outlook” reveals that the global energy demand is expected to grow by 30%, fossil fuels are predicted to dominate the world energy in the next 20 years, accounting for at least three-quarters of energy supply (BP, 2017a), and oil still remains as the leading fuel, accounting for a third of global energy consumption (BP, 2017b). Enhancing oil recovery (EOR) from the existing fields is considered as a key technology to meet the need, and calls for better understanding of pore-scale physical processes that are responsible for trapping of oil in pore space of reservoir rocks in presence of other reservoir fluids. Recent advance in X-ray Computed Tomography (CT) has made it possible to observe fluid phase displacements in the pore structures of real reservoir rock samples. As a result, CT has now become an indispensable tool to understand competing phase

displacement mechanisms and to characterize fluid phase configurations in laboratory setups that mimic reservoir in-situ conditions and reservoir operational conditions (Sedgwick and Miles-Dixon, 1988). There has been a surge of applications of CT technology in this specific area (Bekri et al., 2005; Arns et al., 2007; Yao et al., 2013; Yang et al., 2015, 2016a, 2016b; Arzilli et al., 2016), and this trend is expected to continue along with the improvement of CT technology and experimental techniques to study fluid phase displacements in more geologically complex reservoirs (e.g., high-temperature and high-pressure reservoir).

In EOR, morphology, configuration and migration of the remaining oil at a high water-cut are of primary concern in oil field development. CT has been widely used to observe multiphase fluid flow in rock (Auzerais et al., 1991; Akin and Kovscek, 1999; Akin et al., 2000; Krummel et al., 2013;

*Corresponding author. E-mail: yangyongfei@upc.edu.cn

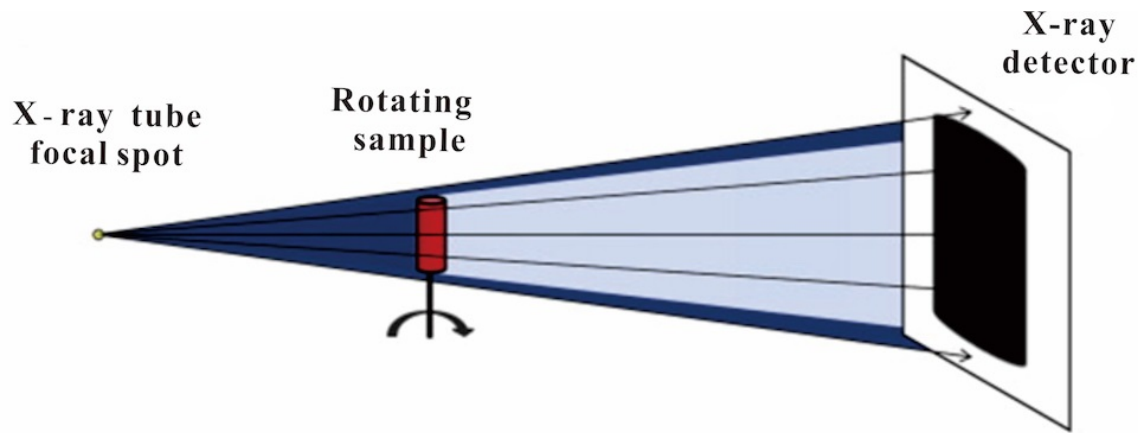


Fig. 1. Schematic diagram of a typical lab-based micro-CT setup with a conical X-ray beam that allows geometrical magnification (Cnudde and Boone, 2013).

Wildenschild and Sheppard, 2013; Berg et al., 2014; Pak et al., 2015; Norouzi Apourvari and Arns, 2016; Tsuji et al., 2016). The quantitative characterization of flow through a porous medium was carried out (Auzerais et al., 1991), a systematic investigation of fluid flow characteristics within diatomite was performed using CT (Akin et al., 2000), the effect of the pore size distribution on the displacement efficiency of multiphase flow in porous media was studied (Yang et al., 2016a), and the multiphase-flow properties of fractured porous media were studied using a laboratory flow apparatus in fractured sandstone systems (Rangel-German et al., 2006), these are the foundation for the quantitative characterization of remaining oil.

The remaining oil in the swept zone of a displacement is often taken as the target oil for enhanced recovery processes (Chatzis et al., 1983). However, what kind of distribution of remaining oil generally appears, and what kind of remaining oil has potential for exploitation, need to be further studied. Therefore, a thorough understanding of transport properties in porous materials and their dependence on pore geometry is critical (Cai et al., 2010, 2017a, 2017b; Wei et al., 2015). Several measurements of the oil cluster distribution have been performed in many papers. In the earliest studies, clusters of all size were observed, with approximately power-law distributions (Iglauer et al., 2012). It had been found that cluster size can range from a single pore to multiple-pore configurations (Karpyn et al., 2010; Kumar et al., 2010; Iglauer et al., 2013). The blob size was directly related to the viscous force, and the blob surface area and volume had an impact on the mass transfer characteristics of the system (Al-Raoush and Willson, 2005). More recently, a tendency for remaining non-wetting-phase saturations to increase as the porosity decreased was noted. This was related to a strong relationship between trapping and aspect ratio (Al-Raoush, 2014). The trapping oil has been measured in pore-scale experiments, but these do not obtain a consistent understanding of morphology change of trapped cluster.

Our study uses the core of the oil field, with the help of CT, to conduct the oil-water displacement experiments in quasi-real time. In this process, the internal structure of the core

will not be changed, and then, we can understand the forming mechanism and distribution pattern of microscopic remaining oil, as well as visually display the oil-water distribution of the different displacement processes at the microscopic scale to provide a basis for tapping the potential of remaining oil.

2. Construction of a digital core based on CT scanning

2.1 CT scanning method

The CT equipment is mainly composed of the following three parts: a. the scanning part, including the X-ray source, detector and scanning frame; b. computer system to store and work with the collected scanning data; and c. image displaying and storage system.

The principles of μ -CT scanning have been thoroughly described by Cnudde and Boone (2013) are shown in Fig. 1, where the X-ray source emits radiation to pass through the sample; the intensity of the X-ray will decay. Then, the signal is received by the detector. Finally, the received signal is processed. From a mathematical perspective, Kak Avinash C et al. and Natterer et al. described the mechanism of CT in detail (Kak and Slaney, 2001; Natterer, 2001; Kak et al., 2002).

And the applications of μ -CT are wide, including digital core analysis and pore-network modeling (Arns et al., 2007; Carpenter, 2015); machined fragments of a number of core plugs using a high resolution X-ray micro-computed tomography (micro-CT) facility (Arns et al., 2005); pore-scale imaging and modeling for digital core analysis (Blunt et al., 2013), REV identification (Gao et al., 2014), which make great contributions on constructing and analyzing the digital core.

The CT machine used in this paper is the MicroXCT-400 machine from the China University of Petroleum (East China).

2.2 CT scan of a dry rock sample

In order to determine the initial pore space and to prepare for the image segmentation when the core is saturated by fluid,

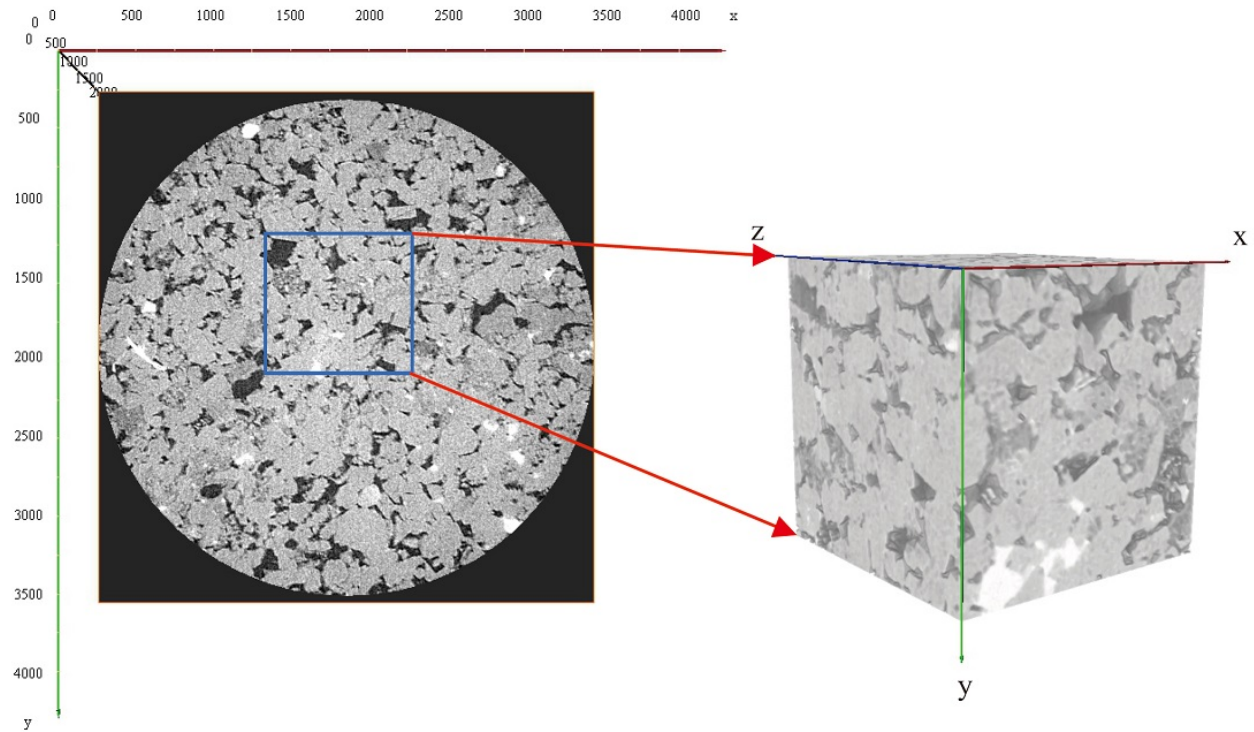


Fig. 2. Reconstructed gray digital core (the resolution of the fine scan is $3.78 \mu\text{m}/\text{pixel}$); the left 2D picture ($1024 \times 1024 \text{ pixels}^2$) is a slice of the 3D core sample, the size of the 3D extracted subvolume is $1.13 \text{ mm} \times 1.13 \text{ mm} \times 1.13 \text{ mm}$.

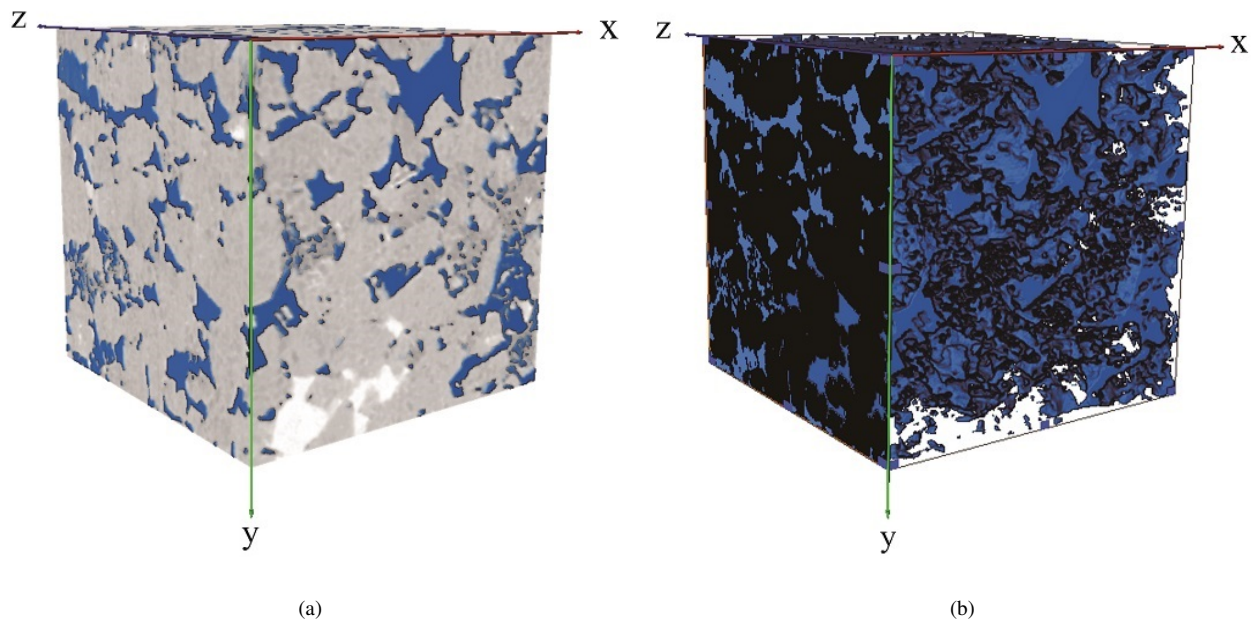


Fig. 3. Three dimensional digital core (the gray is the skeleton, the blue is the pore phase; the skeleton phase is eliminated in (b)); the size is $1.13 \text{ mm} \times 1.13 \text{ mm} \times 1.13 \text{ mm}$.

Table 2. Core sample data.

Core name	Length (mm)	Gas permeability (mD)	Porosity (%)	Diameter (mm)	Volume (mm^3)
7-3-2#	27.1	430.03	22.76	9.0	1723.2

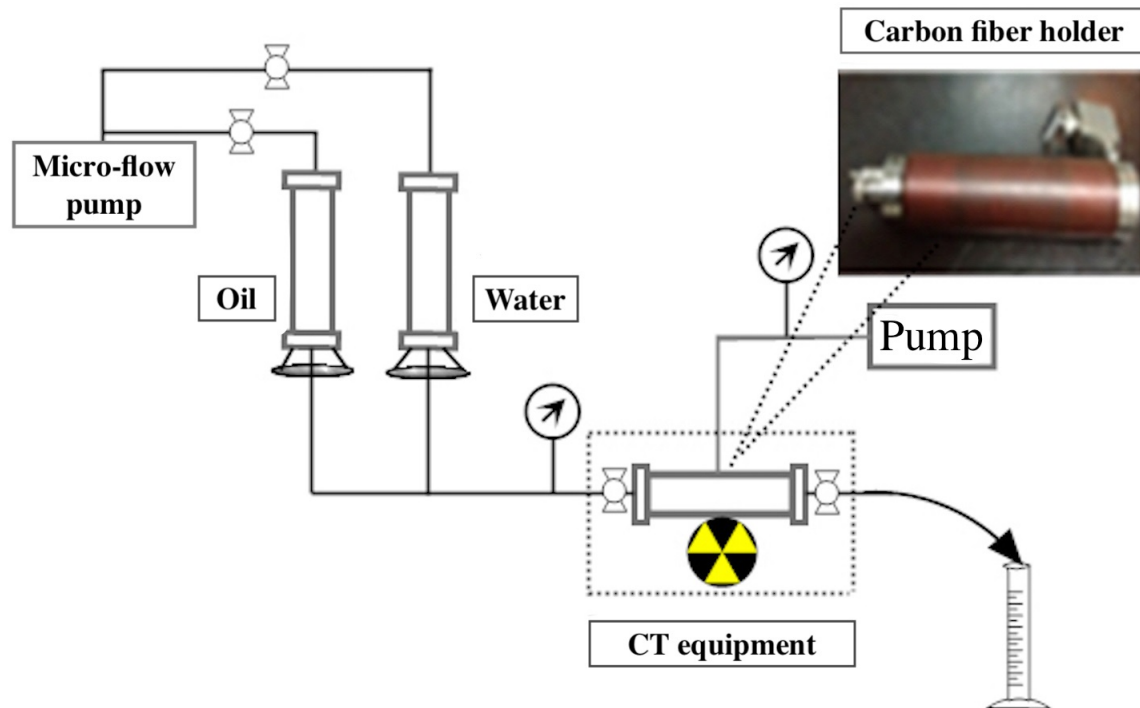


Fig. 4. Installation flow chart of laboratory equipment.

we scan the dry rock sample first.

Take the 7-3-2# core and place the core into a thermostat at a constant temperature of 100 °C for 24 hours so that it fully dries. Place the core into a core holder; CT scanning is used to obtain an accurate and complete pore structure of the dry core (Ioannidis et al., 1995; Hou et al., 2007; Hajizadeh et al., 2011; An et al., 2016; Bultreys et al., 2016; Yang et al., 2016a). It is important to note that the scanning resolution of this study is 3.78 $\mu\text{m}/\text{pixel}$, and the reconstructed 3D gray digital core is shown in Fig. 2.

2.3 Constructing digital cores of pores based on CT scanning

For the three-dimensional gray-scale images shown in Fig. 2, image processing is performed by software (Ioannidis et al., 1995; Hou et al., 2007; Xu et al., 2013; Shah et al., 2016), and the middle rectangular portion is extracted as the study area.

First, the images are denoised and smoothed, and this is favorable for distinguishing between oil and water. Then, segment the images to obtain the oil and water distribution for each section, and further visualize the three-dimensional distribution of oil and water.

Based on this, the corresponding three-dimensional digital core is constructed, as shown in Fig. 3. To strengthen the recognition degree of the pores, the skeleton phase is eliminated, and the result is shown in Fig. 3(b).

By calculating, we know that the porosity and the permeability of the digital core are 20.7% and 412.4 mD respectively, and its comparatively close to the measured porosity in Table

2.

3. Experiment of oil-water displacement over quasi-real time

The experimental apparatus are shown in Fig. 4. To control the influence of the external conditions (mainly temperature) on the experiment, this study controls the temperature at 24 °C. This study also uses a special carbon-fiber core holder with the corrosion resistance and a low density. The most important feature is that the X-ray penetration is good, which produces high quality images during the entire experiment.

3.1 Preparation for the experiment

(1) Preparation of simulated oil. When the temperature is 24 °C, equilibrate the simulated oil viscosity with that of oil from the reservoir.

(2) Brine mixing. Reference the salinity of the reservoir formation water, by using distilled water to adjust the salinity of the NaHCO_3 type brine solution to 12,600 mg/L. The composition of the simulated formation water is shown in Table 1.

Besides, the iodide ion can help for the separation of water phase and oil phase, so we used KI with a mass fraction of 10%. KI has higher relative molecular weight and X ray attenuation coefficient, which can improve the contrast of water phase and oil phase in the images.

(3) Core processing. In this experiment, we carry out washing and drying of the 7-3-2# core first, and then followed with cutting and flattening of the cutting face. Additionally, ph-

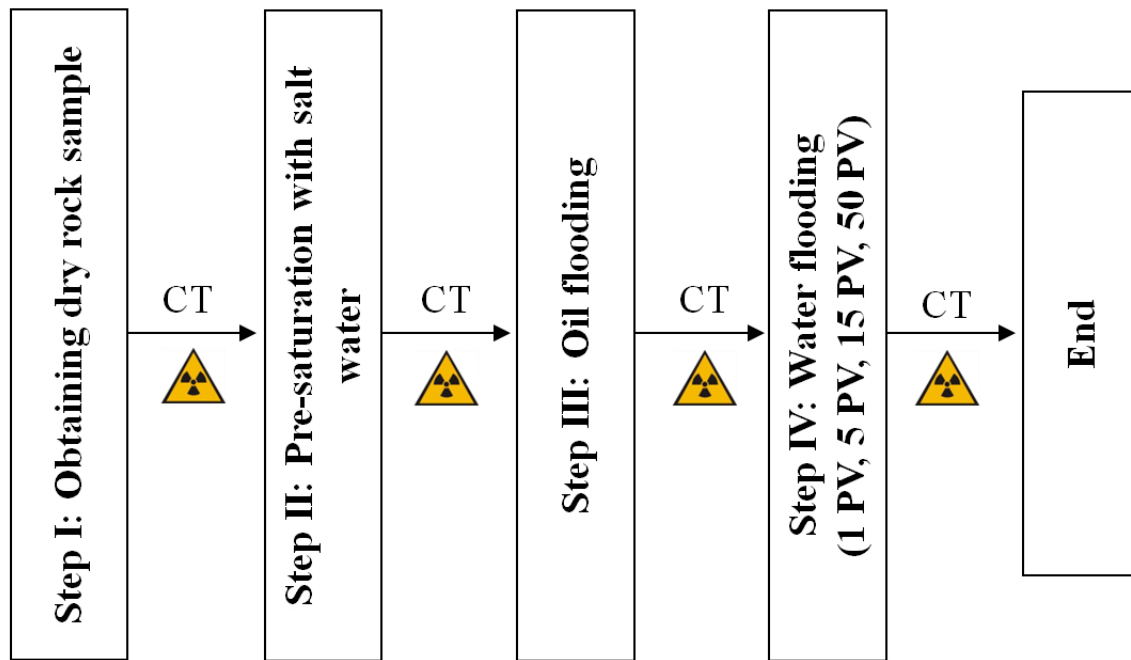


Fig. 5. Experimental flow chart.

Table 1. Simulated formation water composition.

Total mineralization, mg/L	10,700
Viscosity, mPa·s	1.2
Water type	NaHCO ₃
HCO ₃ ⁻ , mg/L	2,000
Cl ⁻ , mg/L	4,312.24
SO ₄ ²⁻ , mg/L	960
Ca ²⁺ , mg/L	45.3
Mg ²⁺ , mg/L	33.5
K ⁺ + Na ⁺ , mg/L	5,257.77

ysical measures on the core length and other basic data were taken. The results are shown in Table 2.

3.2 Experimental process

The experimental process is shown in Fig. 5.

Step I: Scanning dry rock sample; this step was completed in section 2.2.

Step II: Pre-saturation, allows the core to be saturated by salt water to simulate the original state when the reservoir is not invaded by oil. After the end of the pre-saturation, the core is scanned. At this point, the only fluid in the core is water, which helps to separate and identify the remaining oil for the subsequent steps.

Step III: Oil flooding, i.e., simulation of reservoir forma-

tion, when oil flooding is completed, simulate the oil aging stage and use the results to restore the wettability of the rock. When the aging is complete, CT is used to scan the core.

Step IV: Water flooding simulates the oil field production process. Experiments were carried out at a small step size, and the quasi-real-time images were scanned after 1 PV, 5 PV, 15 PV, 50 PV (residual oil). After the start of the experiment, read and record the pressure and volume of the fluid every 30 minutes.

4. Results and discussion

4.1 Experimental core data

The basic data for the experimental core, as shown in Fig. 6, are as follows: the core diameter is 9.0 mm, length is 27.1 mm, volume is 1,723.2 mm³, dry weight is 4.003 g, wet weight is 4.421 g. Its easy to calculate the porosity measured by water, and the porosity is 22.17%, which is very close to the value 22.76% in the Table 2. This shows that the rock is fully saturated with water.

4.2 Three-dimensional remaining oil distribution

When oil flooding is performed, the oil and water distributions of the core are determined, as shown in Fig. 7 (the size of the 3D extracted subvolume is 1.13 mm×1.13 mm×1.13 mm). The pore space is almost completely filled with oil, and the saturation of bound water is 25.8%.

According to the CT scanning results of water flooding, the distributions of oil and water in the core are reconstructed with 1 PV, 5 PV, 15 PV and 50 PV injection multiples. The results are shown in Fig. 8. By observing the 3D distribution



Fig. 6. 7-3-2# core sample from the oilfield.

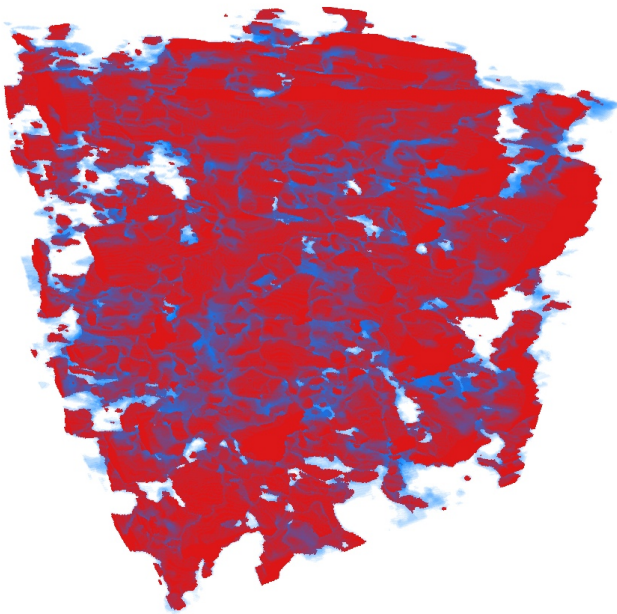


Fig. 7. Oil and water distributions of core 7-3-2# (the size of the 3D extracted subvolume is 1.13 mm×1.13 mm×1.13 mm).

of oil and water in the core, it is easy to show that with the progress of water flooding, the total volume of oil decreases, the state of which is changed from a continuous phase to a dispersed phase, and the remaining oil is minimal after flooding.

4.3 Dynamic evolution and quantitative analysis of the remaining oil

4.3.1 Quantitative characterization of remaining oil

The remaining oil is divided into non-connected pieces,

and the volume and area of the remaining oil are calculated in different injection multiples.

(1) The number of remaining oil blobs at different displacement times shows the dispersion degree of the remaining oil in different injection multiples. Calculating the single blob volume of the remaining oil so that the percentage of different forms of the remaining oil can be calculated (Al-Raoush and Willson, 2005), i.e., the proportion of the network and porous, isolated and film shapes with different degrees of water flooding is calculated.

(2) By calculating the average volume of the remaining oil clusters, it is possible to understand the effect of water injection on the microscopic displacement of the remaining oil.

$$\bar{V} = \sum_{i=1}^n V_i \quad (1)$$

In Eq. (1), \bar{V} is the average volume of the remaining oil in the single blob, n is the number of remaining oils in the study area, and V_i is the remaining oil volume of the i th blob.

4.3.2 Classification of different types of remaining oil

From the reconstructed images, it is not difficult to see, at different displacement times, that there are variable forms of remaining oil. Thus, the three-dimensional shape factor G is used to determine the quantitative distribution, and the computation equation is shown in Eq. (2) (Prodanovi et al., 2007). The microscopic morphology of the remaining oil is divided into network, porous, isolated and film shape, as shown in Table 3.

$$G = \frac{6\sqrt{\pi}V}{S^{1.5}} \quad (2)$$

In Eq. (2), S is the surface area of the single remaining oil and V is the volume of remaining oil.

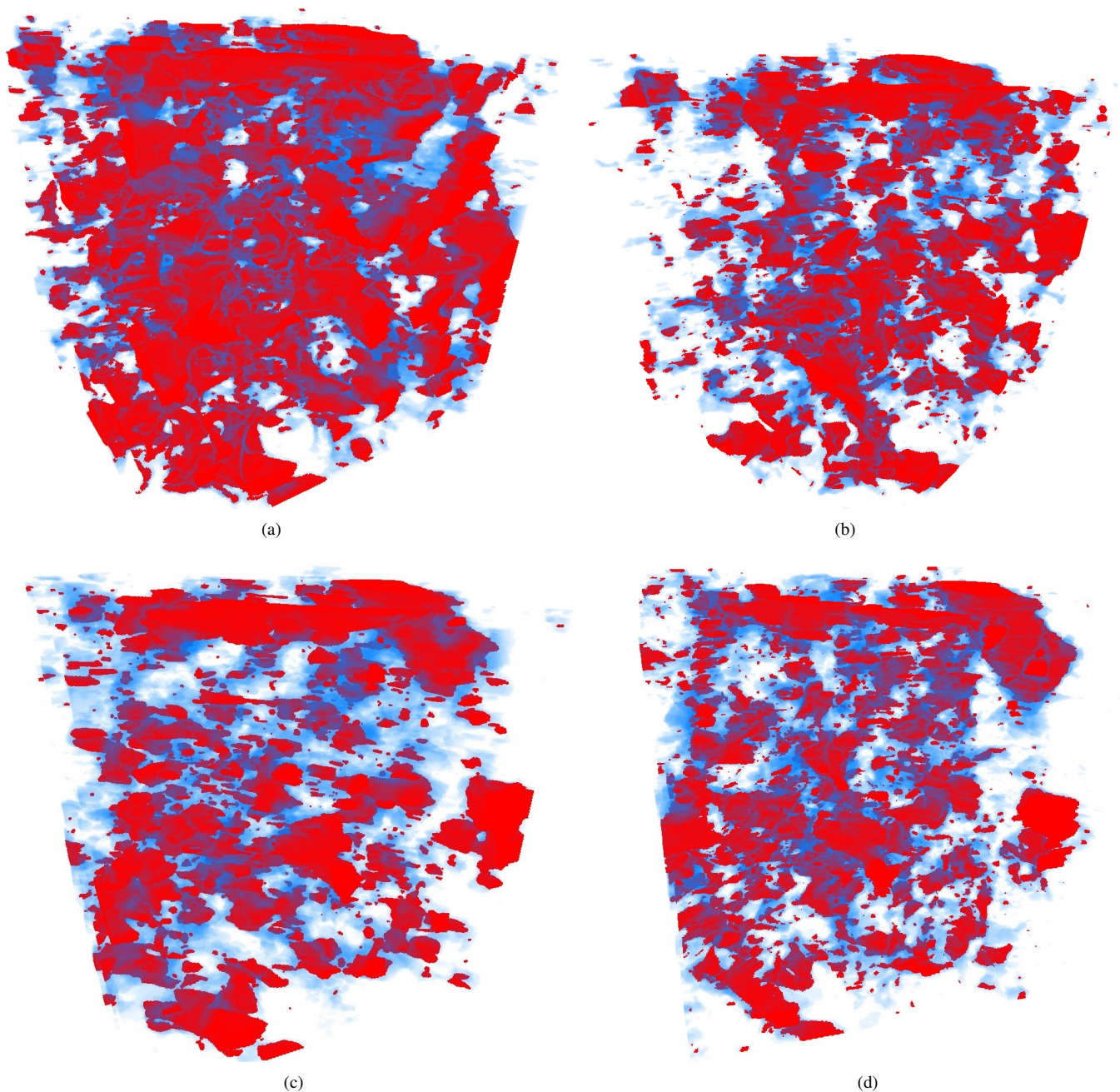


Fig. 8. 3D distribution of the remaining oil in different flooding stages (the size of 3D extracted subvolume is 1.13 mm×1.13 mm×1.13 mm).

Table 3. Range of shape factor G .

Remaining oil type	Range of shape factor G
network	$G < 0.01$
porous	$0.01 < G < 0.1$
isolated	$0.1 < G < 0.3$
film shape	$G > 0.3$

The remaining oil in the network and porous forms is shown in the Fig. 9.

The remaining oil of isolated form (a) and oil film form

(b) is shown in Fig. 10.

4.3.3 Dynamic evolution of the three-dimensional remaining oil distribution

The distribution of remaining oil is analyzed after the core is saturated with oil. It is not difficult to find that with continuous water flooding, the form of remaining oil changes constantly. Initially (when the core is saturated with oil), the remaining oil is mainly composed of large network-like clusters. With continuous water flooding, the network-like remaining oil continues to decrease and changes to a porous shape. Ultimately, the shape changes to isolated and thin oil-

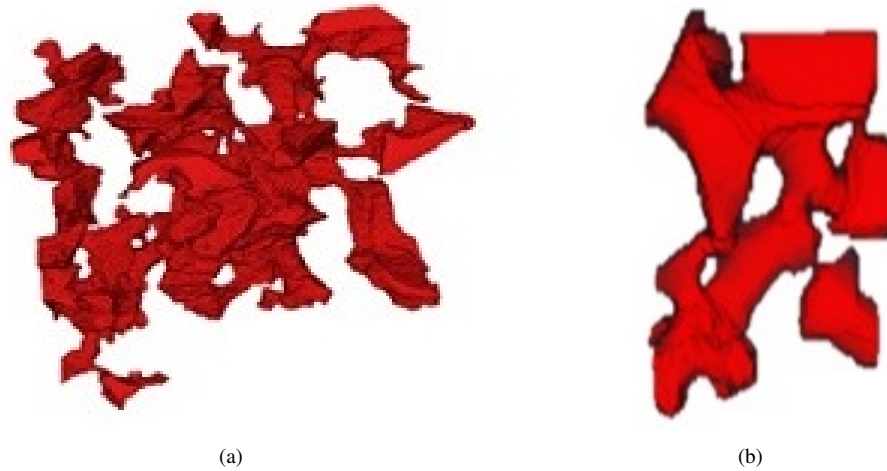


Fig. 9. Remaining oil of network form (a) and porous form (b).

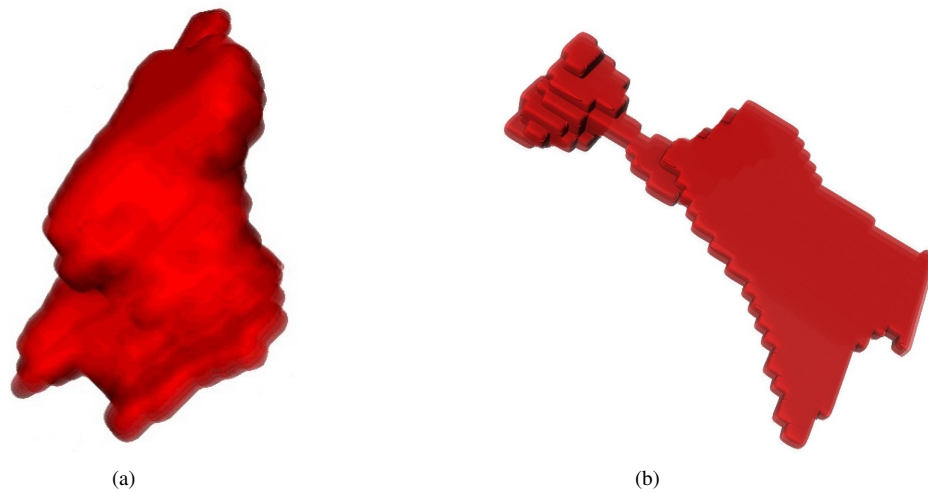


Fig. 10. Remaining oil of isolated form (a) and oil film form (b).

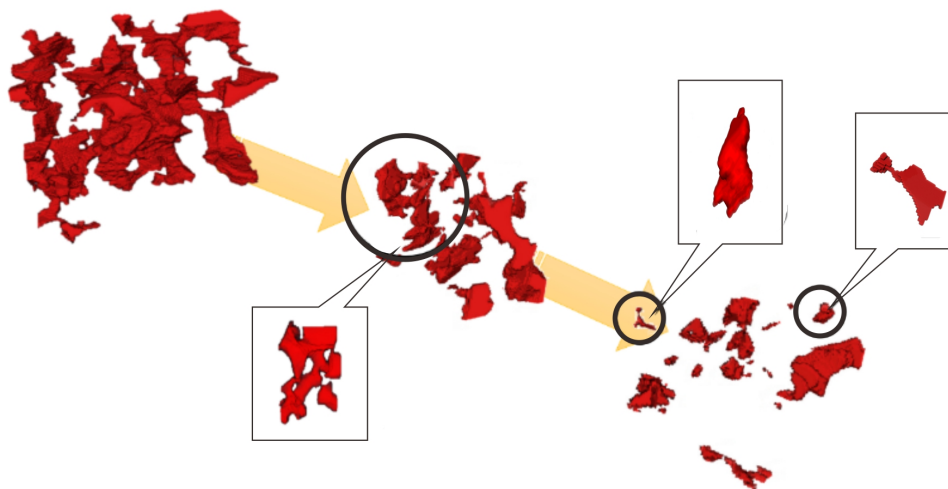
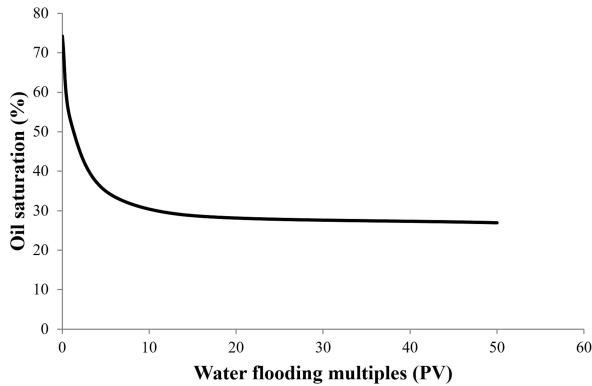


Fig. 11. Evolution process of the three-dimensional remaining oil distribution.

Table 4. Change of the saturation and displacement efficiencies.

Water flooding time	Oil saturation, %	Oil displacement efficiency, %
Saturated oil	74.2	Saturated oil
1 PV	52.3	29.5
5 PV	34.9	53.0
15 PV	28.7	61.3
50 PV	26.9	63.7

**Fig. 12.** Variation of oil saturation with water injection multiples.

film shapes, which are difficult to displace. The dynamic evolution of the remaining oil distribution is simply shown in Fig. 11.

(1) Change of the remaining oil saturation

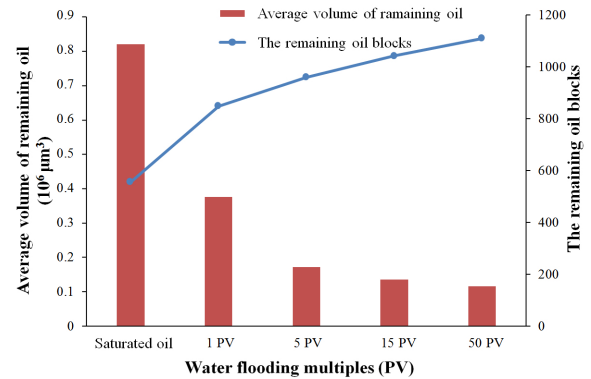
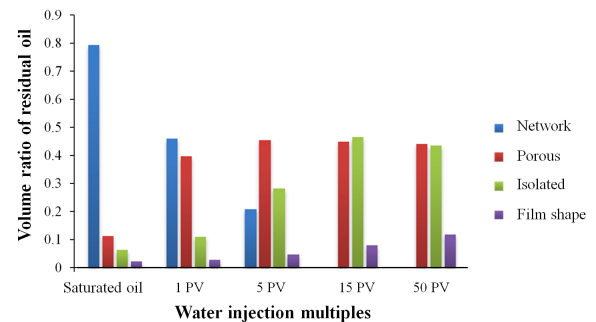
The remaining oil saturation and oil displacement efficiency changes are shown in Table 4 and Fig. 12; it is easy to observe that the initial oil saturation is high. With continuous water flooding, oil saturation decreases significantly. After displacement of 10 PV, the value decreases slowly. At the displacement of 50 PV, the remaining oil is almost impossible to displace; thus, the saturation of residual oil is 26.9%.

(2) Number of remaining oil blobs and the average volume at different injection multiples

It is not difficult to see from Fig. 13 that by increasing the water injection multiples, the remaining oil blobs also increased. Initially, there are 556 remaining oil blobs, but at the displacement of 50 PV, the remaining number of oil blobs increases to 1,109. By contrast, the average volume of remaining oil decreases with increasing water injection multiples. This decrease is significant before 5 PV, it is very slow in the later period, and the total displacement efficiency is 85.1%.

(3) Distribution of remaining oil in different forms

From Fig. 14, according to the volume ratio distribution of different forms of remaining oil, it can be seen that, initially, the forms of the oil mainly become network shape. With continuous water flooding, the network-like remaining oil continues to decrease and change to a porous shape. At 15 PV, the network-like remaining oil disappears and transforms

**Fig. 13.** Change of the remaining oil average volume and blob number.**Fig. 14.** Volume ratio of the remaining oil distribution in different forms.

into isolated and film-like forms that are difficult to displace. At 50 PV, the remaining oil is mainly porous and isolated, with some film-like remaining oil.

The remaining oil in the form of a network mainly appears before the water flooding period; its volume is larger than that of other shapes of the remaining oil, and its structure is more complex. With continuous water flooding, the network-like remaining oil will decrease and even disappear. The remaining oil in the network and porous forms is shown in the Fig. 9. When water flooding begins, the network-like remaining oil breaks up, and with continuous water flooding, the remaining oil presents mainly porous shape.

Isolated remaining oil generally refers to the remaining oil present in single pore that is difficult to reach with water. However, due to water flooding and the effect of water on formation, some of the remaining oil can be reached. Oil-film

shape remaining oil, referring to the remaining oil attached to a rock surface in the form of oil film, is also difficult to mine. Remaining oil of isolated form (a) and oil film form (b) is shown in Fig. 10.

5. Conclusions

- 1) Through CT technology, we carry out a quasi-real time experiment of oil and water flooding. With the premise of not destroying the internal structure of the core, the distributions of different fluids in the pores are obtained by scanning the core. The three-dimensional reconstruction technique is used to reconstruct water and remaining oil in different forms to intuitively simulate the water and oil distributions of the whole process from the beginning to the high water cut.
- 2) The remaining oil of a single blob is taken as the research object, and the volume and surface area of single remaining oil at each displacement time are calculated. According to the statistical results, the remaining oil blobs increase with the increasing of water injection multiples. Initially, the remaining oil blobs are total 556, but at a displacement of 50 PV, the number of remaining oil blobs increases to 1,109. By contrast, the average volume of remaining oil decreases with increasing water injection multiples. The decrease is significant before 5 PV; it is very slow in the later period, and the total displacement efficiency is 85.1%.
- 3) Through the volume ratio distribution of different forms of remaining oil, it can be seen that, initially, the forms of the oil mainly present network shape. With continuous water flooding, the network-like remaining oil continues to decrease and changes to porous shape. At 15 PV, the network-like remaining oil disappears and transforms into isolated and film-like forms that are difficult to displace. At 50 PV, the remaining oil is mainly porous and isolated, with some film-like remaining oil.

Acknowledgments

We would like to express appreciation to the following financial support: The National Natural Science Foundation of China (Nos. 51674280, 51711530131, 51490654 and 51234007). Applied basic research projects of Qingdao innovation plan (16-5-1-38-jch), the Fundamental Research Funds for the Central Universities (No. 17CX05003), National Science and Technology Major Project (2016ZX05010002005), Program for Changjiang Scholars and Innovative Research Team in University (IRT_16R69), and Introducing Talents of Discipline to Universities (B08028).

Open Access This article is distributed under the terms and conditions of the Creative Commons Attribution (CC BY-NC-ND) license, which permits unrestricted use, distribution, and reproduction in any medium, provided the original work is properly cited.

References

- Akin, S., Kovscek, A. Imbibition studies of low-permeability porous media. Paper SPE 54590 Presented at the SPE

Western Regional Meeting, Anchorage, Alaska, 26-27 May, 1999.

Akin, S., Schembre, J., Bhat, S., et al. Spontaneous imbibition characteristics of diatomite. *J. Pet. Sci. Eng.* 2000, 25(3): 149-165.

Al-Raoush, R.I. Experimental investigation of the influence of grain geometry on residual NAPL using synchrotron microtomography. *J. Contam. Hydrol.* 2014, 159: 1-10.

Al-Raoush, R.I., Willson, C.S. A pore-scale investigation of a multiphase porous media system. *J. Contam. Hydrol.* 2005, 77(1): 67-89.

An, S., Yao, J., Yang, Y., et al. Influence of pore structure parameters on flow characteristics based on a digital rock and the pore network model. *J. Nat. Gas Sci. Eng.* 2016, 31: 156-163.

Arns, C.H., Bauguet, F., Ghous, A., et al. Digital core laboratory: Petrophysical analysis from 3D imaging of reservoir core fragments. *Petrophysics* 2005, 46(4): 260-277.

Arns, J., Sheppard, A., Arns, C.H., et al. Pore-level validation of representative pore networks obtained from micro-CT images. Paper SCA200715 Presented at the Proceedings of the International Symposium of the Society of Core Analysts, Canada, 10-12 September, 2007.

Arzilli, F., Cilona, A., Mancini, L., et al. Using synchrotron X-ray microtomography to characterize the pore network of reservoir rocks: A case study on carbonates. *Adv. Water Resour.* 2016, 95: 254-263.

Auzerais, F., Dussan, V., Reischer, A. Computed tomography for the quantitative characterization of flow through a porous medium. Paper SPE 22595 Presented at the SPE Annual Technical Conference and Exhibition, Dallas, Texas, 6-9 October, 1991.

Bekri, S., Laroche, C., Vizika, O. Pore network models to calculate transport and electrical properties of single or dual-porosity rocks. Paper SCA200535 Presented at the International Symposium of the Society of Core Analysts, Toronto, 21-25 August, 2005.

Berg, S., Ott, H., Klapp, S., et al. Multiphase flow in porous rock imaged under dynamic flow conditions with fast X-ray computed micro-tomography. *Petrophysics* 2014, 55(4): 304-312.

Blunt, M.J., Bijeljic, B., Dong, H., et al. Pore-scale imaging and modelling. *Adv. Water Resour.* 2013, 51(1): 197-216.

BP Energy outlook URL [bp.com/energy outlook](http://bp.com/energy_outlook), 2017a.

BP Statistical review of world energy URL bp.com/statisticalreview, 2017b.

Bultreys, T., Boone, M.A., Boone, M.N., et al. Fast laboratory-based micro-computed tomography for pore-scale research: Illustrative experiments and perspectives on the future. *Adv. Water Resour.* 2016, 95: 341-351.

Cai, J., Wei, W., Hu, X., et al. Electrical conductivity models in saturated porous media: A review. *Earth-Sci. Rev.* 2017a, 171: 419-433.

Cai, J., Wei, W., Hu, X., et al. Fractal characterization of dynamic fracture network extension in porous media. *Fractals* 2017b, 25(2): 1750023.

Cai, J., Yu, B., Zou, M., et al. Fractal characterization of spontaneous co-current imbibition in porous media. *Energy*

- Fuels 2010, 24(3): 1860-1867.
- Carpenter, C. Digital core analysis and pore-network modeling in a mature-field project. *J. Pet. Technol.* 2015, 67 (1):97-99.
- Chatzis, I., Morrow, N.R., Lim, H.T. Magnitude and detailed structure of residual oil saturation. *SPE J.* 1983, 23(2): 311-326.
- Cnudde, V., Boone, M.N. High-resolution X-ray computed tomography in geosciences: A review of the current technology and applications. *Earth-Sci. Rev.* 2013, 123(4): 1-17.
- Gao, Y., Yao, J., Yang, Y., et al. REV identification of tight sandstone in Sulige Gas Field in Changqing Oilfield China using CT based digital core technology. Paper SCA2014036 Presented at the 2014 International Symposium of the Society of Core Analysts, Avignon, France, 8-11 September, 2014.
- Hajizadeh, A., Safekordi, A., Farhadpour, F.A. A multiple-point statistics algorithm for 3D pore space reconstruction from 2D images. *Adv. Water Resour.* 2011, 34(10): 1256-1267.
- Hou, J., Zhang, S., Sun, R., et al. Reconstruction of 3D network model through CT scanning. Paper SPE 106603 Presented at the 69th European Association of Geoscientists and Engineers Conference and Exhibition, London, UK, 11-14 June, 2007.
- Iglauer, S., Fern, M.A., Shearing, P., et al. Comparison of residual oil cluster size distribution, morphology and saturation in oil-wet and water-wet sandstone. *J. Colloid Interface Sci.* 2012, 375(1): 187-192.
- Iglauer, S., Paluszny, A., Blunt, M.J. Simultaneous oil recovery and residual gas storage: A pore-level analysis using in situ X-ray micro-tomography. *Fuel* 2013, 103: 905-914.
- Ioannidis, M., Kwiecien, M., Chatzis, I. Computer generation and application of 3D model porous media: From pore-level geostatistics to the estimation of formation factor. Paper SPE 30201 Presented at the Petroleum Computer Conference, Houston, Texas, 11-14 June, 1995.
- Kak, A.C., Slaney, M. Principles of Computerized Tomographic Imaging. USA, SIAM, 2001.
- Kak, A.C., Slaney, M., Wang, G. Principles of computerized tomographic imaging. *Med. Phys.* 2002, 29(1): 107-107.
- Karpyn, Z.T., Piri, M., Singh, G. Experimental investigation of trapped oil clusters in a waterwet bead pack using Xray microtomography. *Water Resour. Res.* 2010, 46(4): 475-478.
- Krummel, A.T., Datta, S.S., Mnster, S., et al. Visualizing multiphase flow and trapped fluid configurations in a model three-dimensional porous medium. *Aiche J.* 2013, 59(3): 1022-1029.
- Kumar, M., Knackstedt, M.A., Senden, T.J., et al. Visualizing and quantifying the residual phase distribution in core material. *Petrophysics* 2009, 51(51): 323-331.
- Natterer, F. The Mathematics of Computerized Tomography. USA, SIAM, 2001.
- Norouzi, A.S., Arns, C.H. Image-based relative permeability upscaling from the pore scale. *Adv. Water Resour.* 2016, 95: 161-175.
- Pak, T., Butler, I.B., Geiger, S., et al. Droplet fragmentation: 3D imaging of a previously unidentified pore-scale process during multiphase flow in porous media. *Proc. Natl. Acad. Sci. USA* 2015, 112(7): 1947-1952.
- Prodanović, M., Lindquist, W., Seright, R. 3D image-based characterization of fluid displacement in a Berea core. *Adv. Water Resour.* 2007, 30(2): 214-226.
- Rangel-German, E., Akin, S., Castanier, L. Multiphase-flow properties of fractured porous media. *J. Pet. Sci. Eng.* 2006, 51(3): 197-213.
- Sedgwick, G., Miles-Dixon, E. Application of X-ray imaging techniques to oil sands experiments. *J. Can. Pet. Technol.* 1988, 27(02): 104-110.
- Shah, S.M., Gray, F., Crawshaw, J.P., et al. Micro-computed tomography pore-scale study of flow in porous media: Effect of voxel resolution. *Adv. Water Resour.* 2015, 95: 276-287.
- Tsuji, T., Jiang, F., Christensen, K.T. Characterization of immiscible fluid displacement processes with various capillary numbers and viscosity ratios in 3D natural sandstone. *Adv. Water Resour.* 2016, 95: 3-15.
- Wei, W., Cai, J., Hu, X., et al. An electrical conductivity model for fractal porous media. *Geophys. Res. Lett.* 2015, 42(12): 4833-4840.
- Wildenschild, D., Sheppard, A.P. X-ray imaging and analysis techniques for quantifying pore-scale structure and processes in subsurface porous medium systems. *Adv. Water Resour.* 2013, 51(1): 217-246.
- Xu, Z., Teng, Q., He, X., et al. A reconstruction method for three-dimensional pore space using multiple-point geology statistic based on statistical pattern recognition and microstructure characterization. *Int. J. Numer. Anal. Methods Geomech.* 2013, 37(1): 97-110.
- Yang, Y., Liu, P., Zhang, W., et al. Effect of the pore size distribution on the displacement efficiency of multiphase flow in porous media. *Open Phys.* 2016a, 14(1): 610-616.
- Yang, Y., Wang, C., Yao, J., et al. A new voxel upscaling method based on digital rock. *Int. J. Multiscale Comput. Eng.* 2015, 13(4): 339-346.
- Yang, Y., Zhang, W., Gao, Y., et al. Influence of stress sensitivity on microscopic pore structure and fluid flow in porous media. *J. Nat. Gas Sci. Eng.* 2016b, 36: 20-31.
- Yao, J., Wang, C., Yang, Y., et al. Upscaling of carbonate rocks from micropore scale to core scale. *Int. J. Multiscale Comput. Eng.* 2013, 11(5): 497-504.